Article

Thermodynamic Performance of a Cogeneration Plant Driven by Waste Heat from Cement Kilns Exhaust Gases

Baby-Jean Robert Mungyeko Bisulandu [1,2,*], **Adrian Ilinca** [3], **Marcel Tsimba Mboko** [4]
and Lucien Mbozi Mbozi [4]

1   Laboratoire de Recherche en Energie Eolienne (LREE), Université du Québec à Rimouski (UQAR),
    300 Allée des Ursulines, Rimouski, QC G5L 3A1, Canada
2   Institut de Recherche Futuris—Futuris Research Institute (InReF), OEFC & Faculté Polytechnique,
    Université Kongo, Mbanza-Ngungu B.P. 202, Democratic Republic of the Congo
3   Department of Mechanical Engineering, École de Technologie Supérieure, Montreal, QC H3C 1K3, Canada
4   Faculté Polytechnique, Université Président Joseph Kasa-Vubu,
    Boma B.P. 314, Democratic Republic of the Congo
*   Correspondence: baby-jeanrobert.mungyekobisulandu@uqar.ca or jr.bisulandu@gmail.com

Abstract: The dwindling and scarcity of fossil energy sources is the basis of the energy transition, where renewable resources are increasingly valued. The purpose of the cogeneration system studied in this article is to recover the residual heat from the gases coming out of the chimneys of the cement kilns, to produce at the same time the electricity and the heat required for offices and residential houses of cement workers. Cement kilns are reputed to be energy-intensive, generating excessive heat losses. These heat losses are found mainly in the conduction–convective and radiative modes, representing about 26% of the overall heat input to the system. Nevertheless, the gases at the chimney outlet can still have temperatures between 250 and 350 °C, which presents a non-negligible potential for a cogeneration system. This study compares the thermal performance of different cogeneration plant configurations (KCA, KCB, and KCC systems) using the Kalina cycle to determine the best one. Several assumptions were made to reduce the complexity of the model. MATLAB and Excel software were used to solve the system of equations. After extensive analysis of the results, the KCA system showed the best performance, compared to the KCB and KCC systems, with a thermal efficiency of 22.15%, an exergy efficiency of 45.12%, and a net electrical capacity of 2565.03 kWe. Model sensitivity to concentration, temperature, and pressure variations also gave the KCA system the best-performing system. Evaluation of the excess heat flux removed from the process yields values of 7368.20 kW, 7421.86 kW, and 8094.15 kW for the KCA, KCB, and KCC systems. The results of this article serve as a decision support tool for installing the cogeneration system via the Kalina cycle in cement installations.

Keywords: cogeneration plant; exit gases from cement kilns; waste heat recovery; kalina cycles; heat transfer; electrical power

1. Introduction

The cement industry is energy-intensive and one of the industries that evacuate gases at high temperatures [1–3]. This energy comes from the clinker manufacturing process, whose combustion flame from fossil fuels (coal, heavy fuel oil, and natural gas) or alternative fuels (biomass, tires, and RDF) can reach temperatures around 2000 °C. This process generates hot gases, which are evacuated through the chimneys via the preheater tower. However, as these gases still contain significant energy, producing either electrical energy, domestic or industrial cold, or supplying this heat to urban heating networks is possible. This valorization enters well into sustainable development and the ecological and energy transition framework.

Optimizing energy consumption is compulsory at present for dwindling energy resources worldwide. Furthermore, the International Energy Agency (IEA) speaks of a growth rate of energy consumption in the building sector, both residential and non-residential, of 1.3% per year, which is higher than the annual growth rate of the population. As such, this energy consumption will increase from 91 quadrillion Btu in 2018 to over 139 quadrillion Btu in 2050 [4]. Waste heat recovery in industrial processes offers the most significant energy savings opportunity. The heat rejected from industrial processes can be supplied to other industrial facilities with energy deficits [5]. Heat is generally rejected from one system at a higher temperature to another at a lower temperature. In the literature, organic Rankine and Kalina cycles have long been considered for cogeneration or trigeneration in an industrial plant [6–12].

In the present study, the Kalina cycle has been selected considering its proven performance and efficiency in industrial energy recovery. The Kalina cycle was patented in the 1980s [13]. It uses as a working fluid the mixture of water–ammonia, which behaves as a single fluid due to the molar mass values being almost close to 17 kg/mol for ammonia and 18 kg/mol for water. This mixture works under the effect of distillation, i.e., as the temperature increases, the most volatile fluid vaporizes as soon as it reaches its vaporization temperature [13]. The Kalina cycle can also operate at temperatures above 400 °C, making it more efficient than the organic Rankine cycle [13]. For Varma and Srinivas [14] and Júnior et al. [13], the Kalina cycle also improves the thermal efficiency of the ordinary Rankine cycle by 20 to 40%. According to Varma and Srinivas [14], Júnior et al. [13], and Salemi et al. [15], the Kalina cycle is better than the organic Rankine cycle in terms of exergy efficiency, with values of 15–18% compared to 7–10%, respectively, under the same operating conditions. According to Inayat [16], the Kalina cycle is used for high temperatures (in the range of 100 to 450 °C) and can give high efficiencies between 20 and 35%. According to Cheng et al. [17], the Kalina cycle is a promising heat-to-electricity conversion technology for low-grade heat recovery applications. According to Hossain et al. [18], in recent years, the Kalina cycle has seen increasing interest in high-temperature applications (with average working fluid temperatures of 500 °C at the turbine inlet). It is used as an alternative to the conventional steam Rankine cycle.

Many works in the literature deal with waste heat recovery using the Kalina cycle. Da Costa Horta et al. [19] worked on the cogeneration of electricity from waste heat recovery in the cement industry. The purpose of this work was to compare two Kalina cycles in terms of operation and performance characteristics. The results of this study showed that one of the Kalina cycles was more competitive regarding the net power generated. Zheng et al. [20] have undertaken a comparative study of the performance of a dual-pressure Kalina cycle to utilize low-grade geothermal energy. This paper applies the sliding pressure control strategy to respond to variations in geothermal energy parameters. The two-stage evaporation pressures in the parallel dual-pressure Kalina cycle are adjusted to keep constant the temperature difference between the geothermal energy input temperature of the evaporators and the corresponding turbine input temperature. The results found that the proposed parallel double-pressure Kalina cycle performs better in net power output and exergy efficiency than the basic Kalina cycle. Akimoto et al. [21] evaluated an electric power generation system that integrates multiple Kalina cycles and absorption heat pumps. They reported that the absorption heat pump cycle could be used as a cooling unit to improve thermal efficiency and create an efficient cogeneration system. Roeinfard and Moosavi [22] optimized the overall performance of Kalina and Rankine cycles (ORC) in different operating modes using thermodynamic relations and sensitivity analysis. The results showed better performance of the Kalina cycle regarding waste heat recovery, efficiency, and fuel consumption. Salemi et al. [15] undertook a techno-economic study of energy recovery from the waste heat of the MIDREX process by using the Kalina cycle in the direct iron reduction process (Figure 1). The work showed that it was possible to recover an average of 2 MW of electricity via the Kalina cycle with a mixture of ammonia and water. Zhang et al. [23] studied the thermodynamic parameters of a Kalina cogeneration

cycle, aiming to produce electricity and cold at a modulable refrigeration temperature. The system gave thermal and exergy efficiencies of 25.71% and 56.53, respectively, for a heat source temperature of 400 °C. Almatrafi et al. [24] also worked on the thermodynamic parameters of a cogeneration Kalina cycle. As the energy source is solar, the efficiencies found are in the range of 17.68% and 7.85% for thermal and exergy efficiency, respectively.
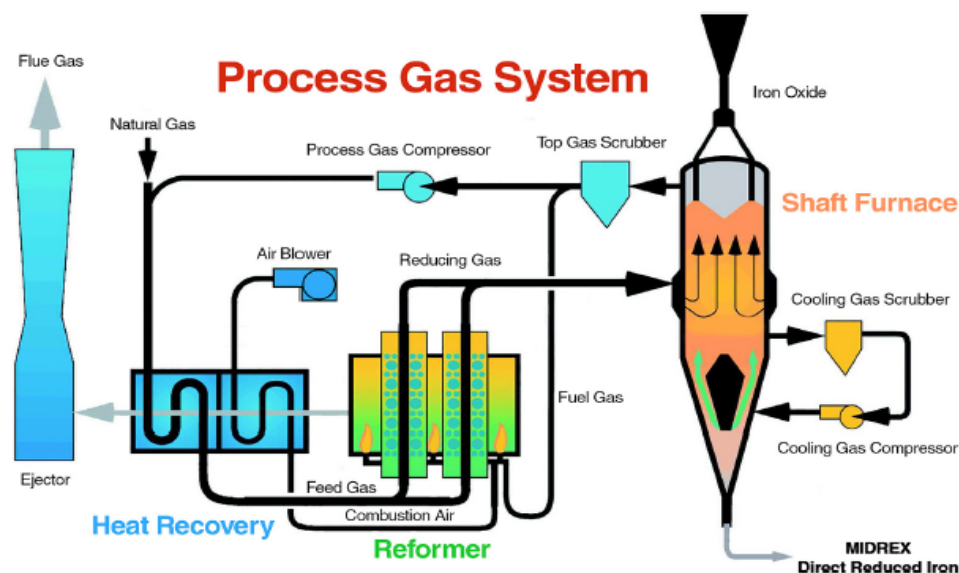

Figure 1. Flowsheet of MIDREX process [15].

Cheng et al. [17] worked on a dynamic model of a Kalina cycle system driven by a low-quality heat source to analyze the system's dynamic behavior. The authors emphasized the importance of the Kalina cycle in the system's dynamic behavior and safe operation due to the fluctuation of the external heat sources. The dynamic behavior of the Kalina cycle system is analyzed by considering disturbances in the control strategy of the valve–pump coordination, in the heat source temperature, the mass flow rate of the heat source, and the system load. Results show the importance of the valve and pump in the design and improvement of the control system. Zhang and Li [25] focused on the thermodynamic performance (i.e., thermal efficiency, network, and exergy efficiency) of Kalina cycles. Zhang and Li [25] conclude that the cycle's thermodynamic performance can be improved by connecting the regenerator and the evaporator in series. Zhu et al. [26] studied the performance improvement of Brayton S-CO$_2$ combinations as working substances of the organic Rankine (ORC) and Kalina cycles. The efficiency and volumetric flow rate ratio were used as a system performance study parameter to evaluate the combined cycle's balance between economy and compactness. The results of this study show that superheating organic working fluids can improve the exergy efficiency of the evaporator and increase $\eta_{orc}/Q_{v,max}$ without an impact on the cycle efficiency. Zoghi et al. [27] used the modified Kalina cycle in a multi-generation biomass system to recover waste heat. The modified Kalina cycle is combined with the gas turbine cycle and the steam Rankine cycle. An expansion valve is used between the two separators and an LNG regasification system. The results show that the modified LNG system has an overall acceptable performance. Hossain et al. [18] presented a model for optimizing the performance of two types of Kalina cycles (Kalina-12A cycle and Kalina-12B cycle) based on the influence of parameters such as ammonia concentration in the working fluid and evaporation pressure. This optimization aims to maximize the multiphase valve's net power output under steady-state operating conditions. As a result, the performances (net power output and thermal efficiency) of these two cycles were improved compared to those of the conventional Kalina cycle. Kalina cycles use several solution types, the preferred one being the ammonia–water mixture [28]. The reasons are, among others, that ammonia and water have approximately the same

weight; the low evaporation temperature of ammonia, and the high performance of water vapor; the ammonia contributes to the efficient use of the heat source at low temperatures and a higher pressure by starting the boiling at a lower temperature (ammonia–water solution has no fixed boiling point, so it is not azeotropic) [28–32].

Based on the studies presented above, the Kalina cycle is pertinent in valorizing the residual heat of the exit gases of the cement plant. Therefore, this paper studies and analyzes the performances of different Kalina cycles for a specific case of cogeneration in the cement industry. This work aims to study the power generation performance and economic efficiency for low-temperature differences, typical for low temperatures of the heat source. Using cogeneration, the proposed integrated system can improve the power production performance by up to 81% over the conventional Kalina cycle. It is also more economical than the conventional Kalina cycle when applied to heat sources above 353 K.

2. Methodology

We consider the energy in the gases coming out of the chimneys of the preheater tower and the clinker cooler to be recovered for a cogeneration system (heat and electricity). The first step was to evaluate the performances of different Kalina cycles for a specific case of cogeneration. The most performant Kalina cycle will be used for the cogeneration system. Those cycles are applied to a case study in the cement installation of Lukala in the Democratic Republic of Congo. The thermodynamic model of Kalina cycles is presented, including energy and exergy analysis and heat exchanger modeling. Then, the validation of the model uses comparative studies for the Kalina cycle operating ranges and results found in the literature. Finally, a conclusion and perspectives on the possibility of adapting to a multi-generation system.

2.1. Description of Kalina Cycles

The heat recovery system in a cyclone tower and in the clinker cooler stack of a rotary cement kiln, whose respective temperatures are above 150 °C, uses the different Kalina cycles to evaluate their performance for electrical energy production. These cycles work as follows (Figure 2). Pump 1 sucks the water–ammonia mixture under atmospheric conditions and sends it to a preheater. The preheated mixture is sent to an evaporator, where it evaporates, and the steam obtained is sent to the first superheater to be superheated. For case (B) in Figure 2, the steam leaving superheater 1 also passes through superheater 2 before being admitted to the high-pressure turbine. The superheated mixture enters the high-pressure turbine, where thermal energy is transformed into kinetic energy at the turbine shaft (for cases (A) and (B), Figure 2). For case (C) in Figure 2, the superheated mixture first passes through a separator, where the steam is sent to the high-pressure turbine, and the liquid phase is collected at the bottom of the separator and then sent to a point where it is mixed with steam leaving the low-pressure turbine. The steam expanded in the high-pressure turbine passes through the second superheater (cases (A) and (C), Figure 2) before its admission in the medium-pressure turbine (case (A), Figure 2) or the low-pressure turbine (case (C), Figure 2). These last steps transform the thermal energy into kinetic energy, driving an electric current generator. Finally, the steam expanded in the medium-pressure turbine goes to the low-pressure turbine and expands. This expansion also contributes to generating electrical energy thanks to the coupling with the generator. At a constant concentration, the steam passes through a heat exchanger or recuperator, where it preheats the mixture from the pump. The mixture leaving the recuperator thus passes through the condenser. The pump then sucks up the condensed mixture, and the operation repeats itself.
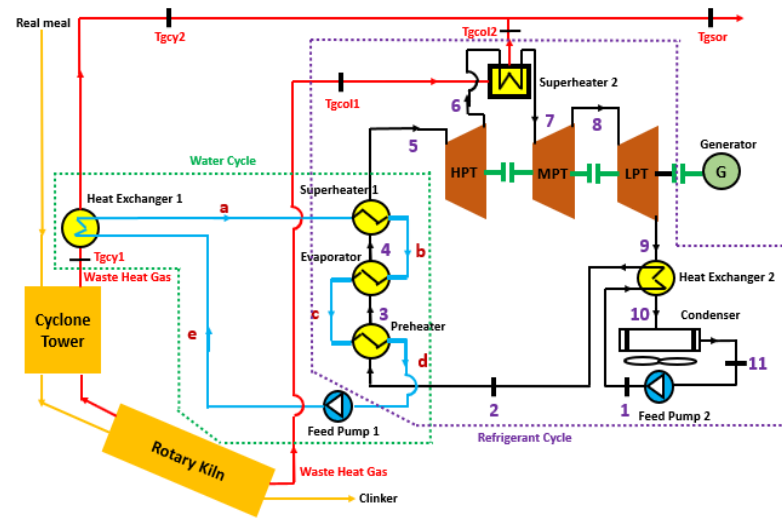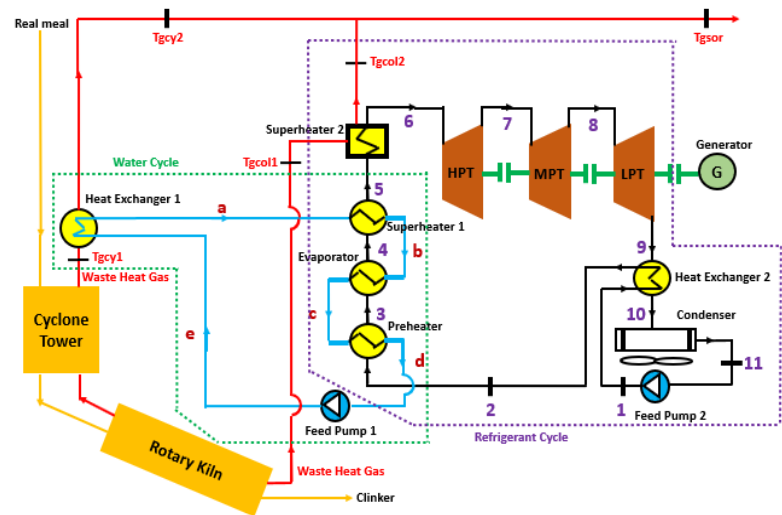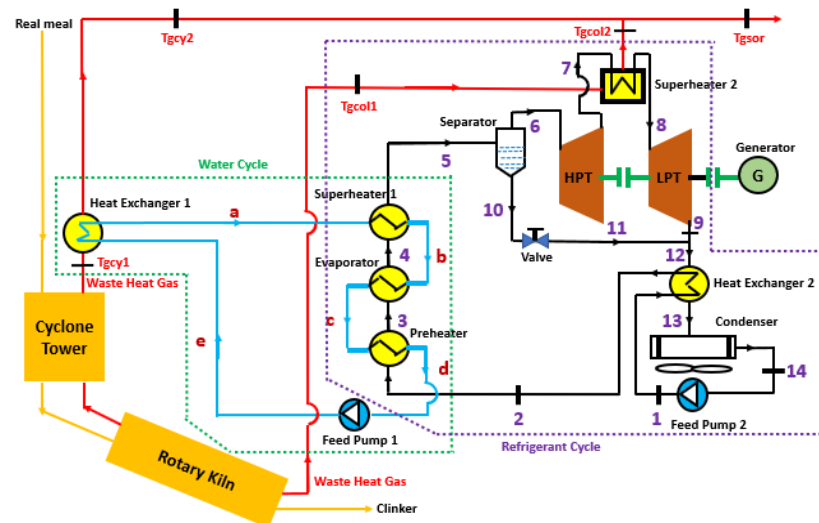
Figure 2. Diagram of Kalina Cycles: (**A**) KCA system, (**B**) KCB system, and (**C**) KCC system.

2.2. Available Energy

The available energy of the exit gases comes from the preheater tower and the chimney of the clinker cooler. It differs according to the industrial process and the type of furnace. The temperature of the gases leaving the preheater tower is an almost standard parameter, depending on the type of furnace. According to Costa Horta [19], there is a restriction on the temperature of the gases leaving the preheater tower. This temperature may not exceed a minimum value, as it is used to dry the raw materials in the crusher.

2.3. Thermodynamic Modeling of Kalina Cycles

Kalina's thermodynamic cycles are modeled, considering energy and exergy balances, energy or isentropic efficiencies, and irreversibility for each component. In addition, the net energy and thermal and exergy efficiencies were calculated for the cycles. The thermodynamic equations of the exchangers, the pump, and the turbines are also established. The concentration of ammonia in the mixture is a crucial parameter in the performance simulation process of the Kalina cycle. The enthalpy balance of the water–ammonia mixture is given as follows:

$$h_{iKalina} = x_{NH3}\, h_{NH3i} + (1 - x_{NH3})h_{H_2O\ i} \tag{1}$$

where $h_{iKalina}$ is the enthalpy of the mixture at point i (i from 1 to the number of points in the cycle, in kJ/kg), x_{NH3} the concentration of ammonia in the mixture (%), h_{NH3i} the enthalpy of ammonia in the mixture at the point i (kJ/kg), and $h_{H_2O\ i}$ the enthalpy of the water vapor in the mixture at point i (kJ/kg).

2.3.1. Data for the Case Study

The different Kalina cycles are tested under the operating conditions of the rotary kiln workshop of the cement plant of Lukala, Democratic Republic of Congo. Values from the industry are used as the operating parameters of the Kalina cycles and are shown in Table 1:

Table 1. Operating parameters of the Kalina cycles.

Operating Parameters	Values
Exit gas temperature (T_{gcy1})	523.15 K
Exit gas mass flow rate	33.33 kg/s
Exit gas temperature of the cooler (T_{gcol1})	573.15 K
Exit gas mass flow rate of the cooler (T_{gcol1})	50 kg/s
Pressure of exit gas (kPa)	1050 kPa
Pressure of cooler exit gas (kPa)	1050 kPa
Turbine isentropic efficiency	85% [11,23,33–39]
Pump isentropic efficiency	85% [11,34,38,40]
Condenser temperature	30 °C
Generator electrical efficiency	98% [35,36]
Generator mechanical efficiency	98% [35,36]
Heat transfer rate of exhausted gas ($\dot{q}_i$)	$\dot{q}_i = h_i A F_i \Delta T_{LMTD}$ [41]
Mass flow rate of working fluid in the water cycle	14.5 kg/s
Mass flow rate of working fluid in Kalina cycle	7.13 kg/s
Ambient temperature	30 °C
Ambient pressure	101.325 kPa
Condenser pinch point temperature difference	10 K [11,15,42]

Table 1. *Cont.*

Operating Parameters	Values
Heat exchanger pinch point temperature difference	10 K [15,33,37]
Temperature of cooling water	20 °C [20]
Concentration of ammonia–water solution	88%
Inlet pressure of the HPT	10,000 kPa
Inlet temperature of the HPT	563.15 K

2.3.2. Main Assumptions

The following hypotheses have been adopted in this article:

- The system is at equilibrium, and the kinetic and potential energies are ignored.
- Pump 1 sucks in at room temperature.
- Mixing of ammonia and water is conducted at room temperature.
- Heat loss was caused by all the power cycle components, and the external environment is neglected.
- The pinch point is 10 K for the superheaters, and the efficiency is 60% for the rest of the exchangers.
- Pumps 1 and 2 draw at the temperature of 30 °C.
- Ammonia-rich vapor and the ammonia-poor solution at the exit of the separator are saturated vapor and liquid, respectively (case (C), Figure 2).
- The concentration at the inlet is 88% for NH_3 and 12% for water.
- Mathematical equations.

Mass and Energy Analysis

The thermodynamic equations for each component in the system are illustrated in the following tables (Tables 2–4). These equations are implemented in MATLAB and Excel.

Table 2. Mass and energy balance of KCA system.

Components	Mass Balance Equations	Energy Balance Equations
Preheater	$\dot{m}_2 = \dot{m}_3$ and $\dot{m}_c = \dot{m}_d$	$\dot{Q}_{preh} = \dot{m}_1(h_3 - h_2) = \dot{m}_a(h_d - h_c)$
Evaporator	$\dot{m}_3 = \dot{m}_4$ and $\dot{m}_c = \dot{m}_b$	$\dot{Q}_{evap} = \dot{m}_1(h_4 - h_3) = \dot{m}_a(h_c - h_b)$
Superheater 1	$\dot{m}_4 = \dot{m}_5$ and $\dot{m}_a = \dot{m}_b$	$\dot{Q}_{superh1} = \dot{m}_1(h_5 - h_4) = \dot{m}_a(h_b - h_a)$
Superheater 2	$\dot{m}_6 = \dot{m}_7$ and $\dot{m}_{gcol1} = \dot{m}_{gcol2}$	$\dot{Q}_{superh2} = \dot{m}_1(h_6 - h_7) = \dot{m}_{gcol}\left(h_{gcol2} - h_{gcol1}\right)$
HPT	$\dot{m}_5 = \dot{m}_6$	$w_{HPT} = h_5 - h_6$
LPT	$\dot{m}_8 = \dot{m}_9$	$w_{LPT} = h_8 - h_9$
MPT	$\dot{m}_7 = \dot{m}_8$	$w_{MPT} = h_7 - h_8$
Heat exchanger 2	$\dot{m}_9 = \dot{m}_{10}$ and $\dot{m}_1 = \dot{m}_2$	$\dot{Q}_{HEX2} = \dot{m}_9(h_9 - h_{10}) = \dot{m}_1(h_2 - h_1)$
Condenser	$\dot{m}_{10} = \dot{m}_{11}$	$\dot{Q}_{cond} = \dot{m}_{10}(h_{10} - h_{11})$
Feed pump 1	$\dot{m}_a = \dot{m}_e = \dot{m}_d$	$w_{pump1} = h_1 - h_{11}$
Feed pump 2	$\dot{m}_{11} = \dot{m}_1$	$w_{pump2} = h_e - h_d$
Heat exchanger 1	$\dot{m}_{gcy1} = \dot{m}_{gcy2}$ AND $\dot{m}_a = \dot{m}_e$	$\dot{Q}_{HEX1} = \dot{m}_{gcy}\left(h_{gcy2} - h_{gcy1}\right) = \dot{m}_a(h_a - h_e)$

Table 3. Mass and energy balance of KCB system.

Components	Mass Balance Equations	Energy Balance Equations
Preheater	$\dot{m}_2 = \dot{m}_3$ and $\dot{m}_c = \dot{m}_d$	$\dot{Q}_{preh} = \dot{m}_1(h_3 - h_2) = \dot{m}_a(h_d - h_c)$
Evaporator	$\dot{m}_3 = \dot{m}_4$ and $\dot{m}_c = \dot{m}_b$	$\dot{Q}_{evap} = \dot{m}_1(h_4 - h_3) = \dot{m}_a(h_c - h_b)$
Superheater 1	$\dot{m}_4 = \dot{m}_5$ and $\dot{m}_a = \dot{m}_b$	$\dot{Q}_{superh1} = \dot{m}_1(h_5 - h_4) = \dot{m}_a(h_b - h_a)$
Superheater 2	$\dot{m}_5 = \dot{m}_6$ and $\dot{m}_{gcol1} = \dot{m}_{gcol2}$	$\dot{Q}_{superh2} = \dot{m}_1(h_6 - h_5) = \dot{m}_{gcol}\left(h_{gcol2} - h_{gcol1}\right)$
HPT	$\dot{m}_6 = \dot{m}_7$	$w_{HPT} = h_7 - h_6$
LPT	$\dot{m}_8 = \dot{m}_9$	$w_{LPT} = h_8 - h_9$
MPT	$\dot{m}_7 = \dot{m}_8$	$w_{MPT} = h_7 - h_8$
Heat exchanger 2	$\dot{m}_9 = \dot{m}_{10}$ and $\dot{m}_1 = \dot{m}_2$	$\dot{Q}_{HEX2} = \dot{m}_9(h_9 - h_{10}) = \dot{m}_1(h_2 - h_1)$
Condenser	$\dot{m}_{10} = \dot{m}_{11}$	$\dot{Q}_{cond} = \dot{m}_1(h_{10} - h_{11})$
Feed pump 1	$\dot{m}_a = \dot{m}_e = \dot{m}_d$	$w_{pump1} = h_1 - h_{11}$
Feed pump 2	$\dot{m}_{11} = \dot{m}_1$	$w_{pump2} = h_e - h_d$
Heat exchanger 1	$\dot{m}_{gcy1} = \dot{m}_{gcy2}$ and $\dot{m}_a = \dot{m}_e$	$\dot{Q}_{HEX1} = \dot{m}_{gcy}\left(h_{gcy2} - h_{gcy1}\right) = \dot{m}_a(h_a - h_e)$

Table 4. Mass and energy balance of KCC system.

Components	Mass Balance Equations	Energy Balance Equations
Preheater	$\dot{m}_2 = \dot{m}_3$ and $\dot{m}_c = \dot{m}_d$	$\dot{Q}_{preh} = \dot{m}_1(h_3 - h_2) = \dot{m}_a(h_d - h_c)$
Evaporator	$\dot{m}_3 = \dot{m}_4$ and $\dot{m}_c = \dot{m}_b$	$\dot{Q}_{evap} = \dot{m}_1(h_4 - h_3) = \dot{m}_a(h_c - h_b)$
Superheater 1	$\dot{m}_4 = \dot{m}_5$ and $\dot{m}_a = \dot{m}_b$	$\dot{Q}_{superh1} = \dot{m}_1(h_5 - h_4) = \dot{m}_a(h_b - h_a)$
Superheater 2	$\dot{m}_7 = \dot{m}_8$ and $\dot{m}_{gcol1} = \dot{m}_{gcol2}$	$\dot{Q}_{superh2} = \dot{m}_1(h_6 - h_5) = \dot{m}_{gcol}\left(h_{gcol2} - h_{gcol1}\right)$
Valve	$\dot{m}_{10} = \dot{m}_{11}$	$\dot{Q}_{valve} = \dot{m}_{10}(h_{10} - h_{11})$
Separator	$\dot{m}_5 = \dot{m}_6 + \dot{m}_{10}$	$\dot{m}_5 h_5 = \dot{m}_6 h_6 + \dot{m}_{10} h_{10}$
HPT	$\dot{m}_6 = \dot{m}_7$	$w_{HPT} = h_7 - h_6$
LPT	$\dot{m}_8 = \dot{m}_9$	$w_{LPT} = h_8 - h_9$
Heat exchanger 2	$\dot{m}_{13} = \dot{m}_{12} = \dot{m}_1 = \dot{m}_2$	$\dot{Q}_{HEX2} = \dot{m}_{12}(h_{12} - h_{13}) = \dot{m}_1(h_2 - h_1)$
Condenser	$\dot{m}_{13} = \dot{m}_{14}$	$\dot{Q}_{cond} = \dot{m}_{13}(h_{13} - h_{14})$
Feed pump 1	$\dot{m}_{14} = \dot{m}_1$	$w_{pump1} = h_{14} - h_1$
Feed pump 2	$\dot{m}_a = \dot{m}_e = \dot{m}_d$	$w_{pump1} = h_e - h_d$
Heat exchanger 1	$\dot{m}_{gcy1} = \dot{m}_{gcy2}$ and $\dot{m}_a = \dot{m}_e$	$\dot{Q}_{HEX1} = \dot{m}_{gcy}\left(h_{gcy2} - h_{gcy1}\right) = \dot{m}_a(h_a - h_e)$

Exergy Analysis

Exergy analysis of a system is based on the first law of thermodynamics [43]. This analysis evaluates the energy transferred and the quality of the exchanged energy. Exergy analysis is helpful for this purpose and investigates the exergy degradation of each system component. So, by applying the exergy relations, it would be possible to consider the modification and mitigation of the exergy degradation to improve system efficiency. By ignoring the changes in kinetic and potential energies, the physical exergy of a flow is defined as [15]:

$$ex_i = (h_i - h_0) - T_0(s_i - s_0) \tag{2}$$

where *s* represents the specific entropy, *i* and 0 subscripts are the flow and initial condition numbers, respectively. The primary exergy relations for each component or equipment are defined as follows [44–48]:

$$\dot{Ex}^{Q} + \sum \dot{Ex}_{In} = \sum \dot{Ex}_{Out} + \dot{Ex}^{W} + \dot{Ex}^{D}$$
$$\dot{Ex}^{Q} = \dot{Q}\left(1 - \frac{T_0}{T_i}\right)$$
$$\dot{Ex}^{W} = \dot{W}$$
$$\dot{Ex}^{D}_{Total} = \sum \dot{Ex}^{D} \qquad (3)$$

The equations for exergy degradation for the main components are presented in Table 5.

Table 5. Exergy degradation balances for the system components.

Exergy Balance Equations			
Components	**KCA System**	**KCB System**	**KCC System**
Preheater	$\dot{Ex}_2 + \dot{Ex}_c = \dot{Ex}_3 + \dot{Ex}_d + \dot{Ex}^{D}_{Preh}$	$\dot{Ex}_2 + \dot{Ex}_c = \dot{Ex}_3 + \dot{Ex}_d + \dot{Ex}^{D}_{Preh}$	$\dot{Ex}_2 + \dot{Ex}_c = \dot{Ex}_3 + \dot{Ex}_d + \dot{Ex}^{D}_{Preh}$
Evaporator	$\dot{Ex}_3 + \dot{Ex}_b = \dot{Ex}_4 + \dot{Ex}_c + \dot{Ex}^{D}_{Evap}$	$\dot{Ex}_3 + \dot{Ex}_b = \dot{Ex}_4 + \dot{Ex}_c + \dot{Ex}^{D}_{Evap}$	$\dot{Ex}_3 + \dot{Ex}_b = \dot{Ex}_4 + \dot{Ex}_c + \dot{Ex}^{D}_{Evap}$
Superheater 1	$\dot{Ex}_4 + \dot{Ex}_a = \dot{Ex}_5 + \dot{Ex}_b + \dot{Ex}^{D}_{Superh1}$	$\dot{Ex}_4 + \dot{Ex}_a = \dot{Ex}_5 + \dot{Ex}_b + \dot{Ex}^{D}_{Superh1}$	$\dot{Ex}_4 + \dot{Ex}_a = \dot{Ex}_5 + \dot{Ex}_b + \dot{Ex}^{D}_{Superh1}$
Superheater 2	$\dot{Ex}_6 + \dot{Ex}_{gcol1} = \dot{Ex}_7 + \dot{Ex}_{gcol2} + \dot{Ex}^{D}_{Superh2}$	$\dot{Ex}_5 + \dot{Ex}_{gcol1} = \dot{Ex}_6 + \dot{Ex}_{gcol2} + \dot{Ex}^{D}_{Superh2}$	$\dot{Ex}_7 + \dot{Ex}_{gcol1} = \dot{Ex}_8 + \dot{Ex}_{gcol2} + \dot{Ex}^{D}_{Superh2}$
HPT	$\dot{Ex}_5 = \dot{Ex}_6 + \dot{w}_{HPT} + \dot{Ex}^{D}_{HPT}$	$\dot{Ex}_6 = \dot{Ex}_7 + \dot{w}_{HPT} + \dot{Ex}^{D}_{HPT}$	$\dot{Ex}_6 = \dot{Ex}_7 + \dot{w}_{HPT} + \dot{Ex}^{D}_{HPT}$
LPT	$\dot{Ex}_8 = \dot{Ex}_9 + \dot{w}_{LPT} + \dot{Ex}^{D}_{LPT}$	$\dot{Ex}_8 = \dot{Ex}_9 + \dot{w}_{LPT} + \dot{Ex}^{D}_{LPT}$	$\dot{Ex}_8 = \dot{Ex}_9 + \dot{w}_{LPT} + \dot{Ex}^{D}_{LPT}$
MPT	$\dot{Ex}_7 = \dot{Ex}_8 + \dot{w}_{MPT} + \dot{Ex}^{D}_{MPT}$	$\dot{Ex}_7 = \dot{Ex}_8 + \dot{w}_{MPT} + \dot{Ex}^{D}_{MPT}$	N.A.
Separator	N.A.	N.A.	$\dot{Ex}_5 = \dot{Ex}_6 + \dot{Ex}_{10} + \dot{Ex}^{D}_{Sep}$
Valve	N.A.	N.A.	$\dot{Ex}_{10} = \dot{Ex}_{11} + \dot{Ex}^{D}_{valve}$
Node	N.A.	N.A.	$\dot{Ex}_{11} + \dot{Ex}_9 = \dot{Ex}_{12} + \dot{Ex}^{D}_{node}$
Heat Exchanger 2	$\dot{Ex}_9 + \dot{Ex}_1 = \dot{Ex}_{10} + \dot{Ex}_2 + \dot{Ex}^{D}_{HEX2}$	$\dot{Ex}_9 + \dot{Ex}_1 = \dot{Ex}_{10} + \dot{Ex}_2 + \dot{Ex}^{D}_{HEX2}$	$\dot{Ex}_{12} + \dot{Ex}_1 = \dot{Ex}_{13} + \dot{Ex}_2 + \dot{Ex}^{D}_{HEX2}$
Condenser	$\dot{Ex}_{10} = \dot{Ex}_{11} + \dot{Ex}^{D}_{Cond}$	$\dot{Ex}_{10} = \dot{Ex}_{11} + \dot{Ex}^{D}_{Cond}$	$\dot{Ex}_{13} = \dot{Ex}_{14} + \dot{Ex}^{D}_{Cond}$
Feed pump 2	$\dot{Ex}_{11} = \dot{Ex}_1 - \dot{w}_{Pump2} + \dot{Ex}^{D}_{Pump2}$	$\dot{Ex}_{11} = \dot{Ex}_1 - \dot{w}_{Pump2} + \dot{Ex}^{D}_{Pump2}$	$\dot{Ex}_{14} = \dot{Ex}_1 - \dot{w}_{Pump2} + \dot{Ex}^{D}_{Pump2}$
Feed pump 1	$\dot{Ex}_d = \dot{Ex}_e - \dot{w}_{Pump1} + \dot{Ex}^{D}_{Pump1}$	$\dot{Ex}_d = \dot{Ex}_e - \dot{w}_{Pump1} + \dot{Ex}^{D}_{Pump1}$	$\dot{Ex}_d = \dot{Ex}_e - \dot{w}_{Pump1} + \dot{Ex}^{D}_{Pump1}$
Heat Exchanger 1	$\dot{Ex}_{gcy1} + \dot{Ex}_e = \dot{Ex}_{gcy2} + \dot{Ex}_a + \dot{Ex}^{D}_{HEX1}$	$\dot{Ex}_{gcy1} + \dot{Ex}_e = \dot{Ex}_{gcy2} + \dot{Ex}_a + \dot{Ex}^{D}_{HEX1}$	$\dot{Ex}_{gcy1} + \dot{Ex}_e = \dot{Ex}_{gcy2} + \dot{Ex}_a + \dot{Ex}^{D}_{HEX1}$

Performance Criteria of Kalina Cycle

The calculations of the performance parameters of a cycle are based on the following:

- Specific network
- Net mechanical power
- Energy and exergy efficiency
- Net electrical power

The thermal power transferred via the superheater is calculated using the formula (4) below [41]:

$$\dot{q}_i = h_i AF_i \Delta T_{LMTD} \qquad (4)$$

For determining the performance of the system (see Table 6), it is essential to define the energy and exergy efficiencies of the waste heat recovery system as follows [15]:

Table 6. Performance criteria of Kalina cycle.

Parameters	Equations		
	KCA System	**KCB System**	**KCC System**
Net Work	$\dot{w}_{net} = \dot{w}_T - \dot{w}_P$		
Energy efficiency	$\eta_{Energy} = \dfrac{\dot{w}_{Net}}{\dot{Q}_{HR} - \dot{Q}_{Rec}}$		
Exergy efficiency	$\eta_{Exergy} = \dfrac{\dot{w}_{Net}}{\dot{Ex}_{In}^{HR}}$		
Pump 2 isentropic efficiency	$\eta_{isPump} = \dfrac{h_{is1} - h_{11}}{h_1 - h_{11}}$	$\eta_{isPump} = \dfrac{h_{is1} - h_{11}}{h_1 - h_{11}}$	$\eta_{isPump} = \dfrac{h_{is1} - h_{14}}{h_1 - h_{14}}$
HPT isentropic efficiency	$\eta_{isHPT} = \dfrac{h_5 - h_6}{h_5 - h_{6s}}$	$\eta_{isHPT} = \dfrac{h_6 - h_7}{h_6 - h_{7s}}$	$\eta_{isHPT} = \dfrac{h_6 - h_7}{h_6 - h_{7s}}$
MPT isentropic efficiency	$\eta_{isMPT} = \dfrac{h_7 - h_8}{h_7 - h_{8s}}$	$\eta_{isMPT} = \dfrac{h_7 - h_8}{h_7 - h_{8s}}$	N.A.
LPT isentropic efficiency	$\eta_{isLHT} = \dfrac{h_8 - h_9}{h_8 - h_{9s}}$	$\eta_{isLHT} = \dfrac{h_8 - h_9}{h_8 - h_{9s}}$	$\eta_{isLHT} = \dfrac{h_8 - h_9}{h_8 - h_{9s}}$

where $\dot{Q}_{HR}$ is the heat recovery in the cyclone and gas cooler. It is given using the following relationship (see Equations (5)–(8)):

$$\dot{Q}_{HR} = \dot{Q}_{HR1} + \dot{Q}_{HR2} \tag{5}$$

with

$$\begin{aligned} \dot{Q}_{HR1} &= \dot{m}_{gcy}\left(h_{gcy1} - h_{gcy2}\right) \\ \dot{Q}_{HR2} &= \dot{m}_{gcol}\left(h_{gcol1} - h_{gcol2}\right) \end{aligned} \tag{6}$$

and

$$\dot{Ex}_{In}^{HR} = \dot{Ex}_{In}^{HR1} + \dot{Ex}_{In}^{HR2} \tag{7}$$

with

$$\begin{aligned} \dot{Ex}_{In}^{HR1} &= \dot{m}_{gcy}\left[\left(h_{gcy1} - h_{gcy2}\right) - T_0\left(s_{gcy1} - s_{gcy2}\right)\right] \\ \dot{Ex}_{In}^{HR2} &= \dot{m}_{gcol}\left[\left(h_{gcol1} - h_{gcol2}\right) - T_0\left(s_{gcol1} - s_{gcol2}\right)\right] \end{aligned} \tag{8}$$

3. Results and Discussions

In this study, the thermodynamic performance analyses are carried out for the Kalina cycles dedicated to cogeneration (simultaneous production of heat and electricity). The result of the thermodynamic performance analysis is summarized in Table 7. This section discusses the energy modeling results of the three Kalina cycles considered under cogeneration conditions. The primary input data for the considered systems are given in Table 1.

Table 7. Performance study parameters of the three cycles studied.

Optimizing Parameters	KCA	KCB	KCC
Net Work [kJ/kg]	367.66	292.15	319.76
Net Mechanical Power [kW]	2817.83	2083.06	2043.12
Net Electrical Power [kWe]	2565.03	2037.43	1998.29
Thermal Efficiency [%]	22.15	18.52	20.93
Exergy Efficiency [%]	45.12	37.26	37.26
Heat flux to be used [kW]	7368.20	7421.86	8094.15

The rejected heat flow is not negligible and can therefore be used in a heat network for factory premises (offices, etc.). Tables 8–10 give the main thermodynamic properties of the KCA, KCB, and KCC systems, respectively. The NH_3 concentration remains constant in the KCA and KCB cycles. However, it varies in the case of KCC. The exergy analysis of the KCC system is shown in Table 11.

Table 8. Thermodynamic properties of KCA system points.

State Point	Mass Flux [kg/s]	Temperature [K]	Pressure [kPa]	Enthalpy [kJ/kg]	Entropy [kJ/kg/K]	Concentration in NH_3 [%]	Volume [m^3/kg]
1	7.13	305.42	10,000	455.57	1.81	88	0.0016
2	7.13	418.24	10,000	1593.62	4.31	88	0.01168
3	7.13	473.15	10,000	1835.28	4.86	88	0.0173
4	7.13	488.15	10,000	1883.14	4.97	88	0.0183
5	7.13	503.15	10,000	1938.36	5.07	88	0.0196
6	7.13	441.33	4340.9	1851	5.27	88	0.0508
7	7.13	563.15	4340.9	2191.11	5.97	88	0.0707
8	7.13	485.05	1884.3	1999.07	6.01	88	0.1391
9	7.13	429.05	818	1897.04	6.01	88	0.2524
10	7.13	354.46	818	1733.81	5.77	88	0.2037
11	7.13	303.15	818	441.8	1.77	88	0.0016

Table 9. Thermodynamic properties of KCB system points.

State Point	Mass Flux [kg/s]	Temperature [K]	Pressure [kPa]	Enthalpy [kJ/kg]	Entropy [kJ/kg/K]	Concentration in NH_3 [%]	Volume [m^3/kg]
1	7.13	305.42	10,000	455.57	1.81	88	0.0016
2	7.13	354.10	10,000	1248.1	3.66	88	0.0062
3	7.13	363.15	10,000	1297.5	3.76	88	0.00702
4	7.13	378.15	10,000	1379.5	3.82	88	0.00841
5	7.13	393.15	10,000	1461.4	4.018	88	0.00981
6	7.13	563.15	10,000	2134.5	5.46	88	0.02415
7	7.13	485.21	4341	1971.6	5.57	88	0.05627
8	7.13	428.11	1884	1890	5.71	88	0.09153
9	7.13	386.56	818	1828.6	5.92	88	0.27959
10	7.13	337.88	818	1713.2	5.61	88	0.19309
11	7.13	303.15	818	441.8	1.77	88	0.0016

Overall, the exergy yields are significantly better than the energy yields (see Table 7). Table 11 shows the exergy destruction for each component at a given evaporating pressure and 0.88 mass fraction of ammonia (KCA and KCB systems) or between 0.88 and 0.90 mass fraction of ammonia (KCC system) of the working fluid. The part of exergy destruction for each component of the different models appears in Figure 3. From the results, Figure 3a shows that the maximum exergy destruction in the KCA system occurs in heat exchanger one (26%), followed by superheater two and the condenser (18%). In contrast, insignificant exergy destruction appears in the pumps, LPT, and superheater one. In the case of the KCB system (Figure 3b), the maximum exergy destruction occurs in heat exchanger one (38%), followed by superheater two (22%), heat exchanger two, and condenser (10%). The pumps, preheater, and superheater one have insignificant exergy destruction. As for

the KCC system (Figure 3c), heat exchangers one and two have high exergy destruction, an estimated share of 22% and 24%, respectively, followed far behind by separator and superheater two, each having shares of 13% and 12%, respectively. In contrast to the two previous cases, the KCC system has a majority of components with low exergy destruction, namely the pumps, valve, condenser, superheater one, HPT, LPT, evaporator, etc.

Table 10. Thermodynamic properties of KCC system points.

State Point	Mass Flux [kg/s]	Temperature [K]	Pressure [(kPa)]	Enthalpy [kJ/kg]	Entropy [kJ/kg/K]	Concentration in NH_3 [%]	Volume [m^3/kg]
1	7.13	305.41	10,000	455.57	1.81	88	0.0016
2	7.13	442.291	10,000	1589.32	4.31	88	0.0146
3	7.13	462.55	10,000	1804.38	4.86	88	0.0167
4	7.13	482.85	10,000	1730.12	4.97	88	0.0183
5	7.13	503.15	10,000	1941.17	5.05	88	0.0199
6	6.2744	503.15	10,000	1925.99	5.27	90	0.0201
7	6.2744	416.98	2860.06	1820.87	5.39	90	0.0759
8	6.2744	563.15	2860.06	2207.88	5.96	90	0.0958
9	6.2744	454.509	818	1979.55	6.34	90	0.0759
10	0.8556	503.15	818	1076.24	6.20	90	0.2694
11	0.8556	450.07	818	1076.24	6.67	10	0.2813
12	7.13	452.29	818	1974.06	5.89	10	0.2485
13	7.13	314.41	818	1643.79	6.16	88	0.2683
14	7.13	303.15	818	441.8	1.77	88	0.1809

Table 11. Exergy analysis of components in Kalina cycle.

Components	Exergy Destruction [kW]			Exergy Efficiency [%]		
	KCA	KCB	KCC	KCA	KCB	KCC
Preheater	2637.58	317.49	2637.58	84.59	98.65	84.59
Evaporator	758.72	730.59	753.72	50.91	55.53	50.91
Superheater 1	790.32	484.74	790.32	65.68	68.76	65.68
Superheater 2	5086.29	5090.65	4434.82	64.55	64.70	43.48
Separator	N.A.	N.A.	5241.80	N.A.	N.A.	23.14
HPT	1159.70	1375.51	1137.15	53.70	84.42	9.24
MPT	1745.38	870.96	N.A.	35.69	66.81	N.A.
LPT	509.47	835.33	560.97	20	52.43	3.05
Valve	N.A.	N.A.	163.82	N.A.	N.A.	91.72
Heat Exchanger 2	3261.88	2261.76	8465.98	79.85	10.70	44.08
Condenser	5332.39	2166.02	2909.21	21.72	35.01	21.79
Feed pump 2	29.34	35.05	35.05	29.88	39.29	35.09
Feed pump 1	8.83	8.83	35.05	88.69	88.69	88.69
Heat Exchanger 1	7456.85	8548.71	7456.85	89.86	57.31	89.86

The temperature versus entropy diagram for KCA, KCB, and KCC are presented in Figure 4A–C, respectively. The green line in subfigures A and B represents the saturation curve for an ammonia concentration of 0.88.
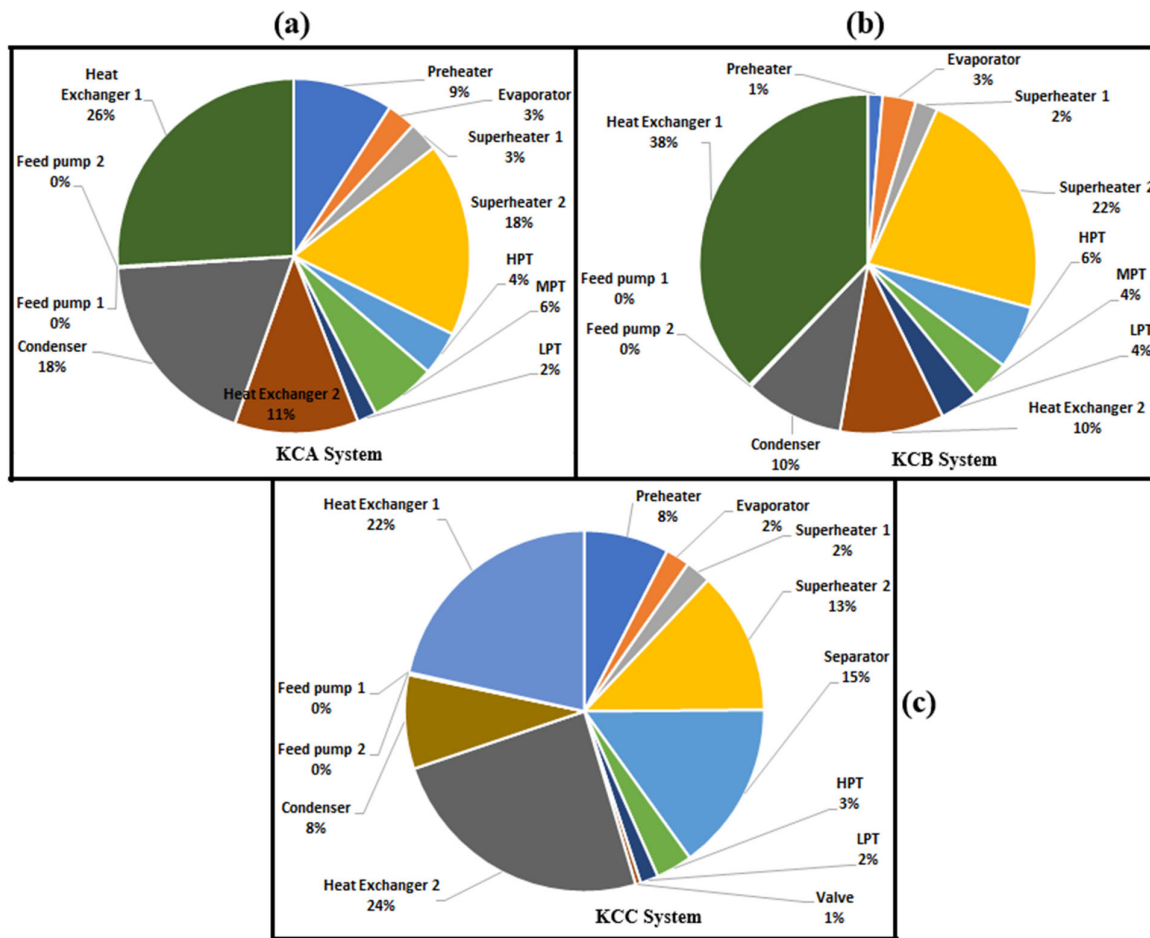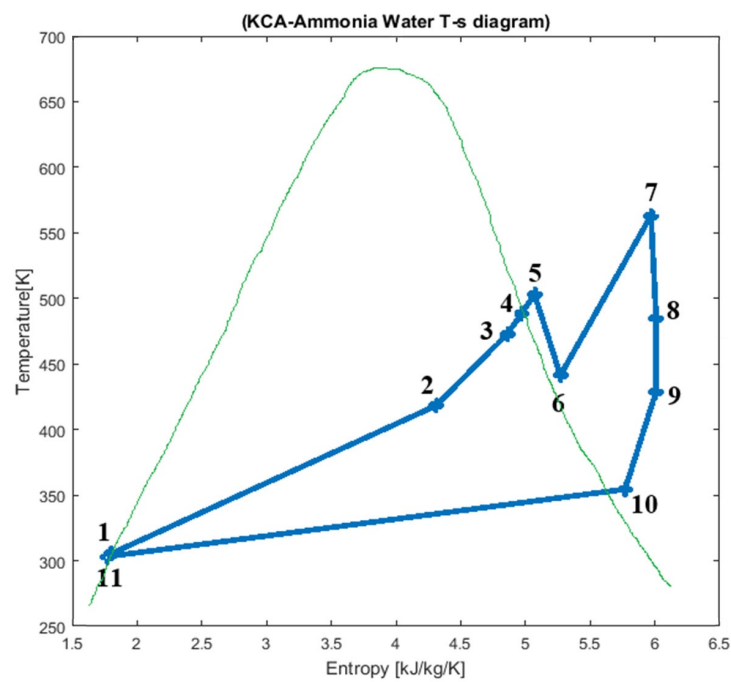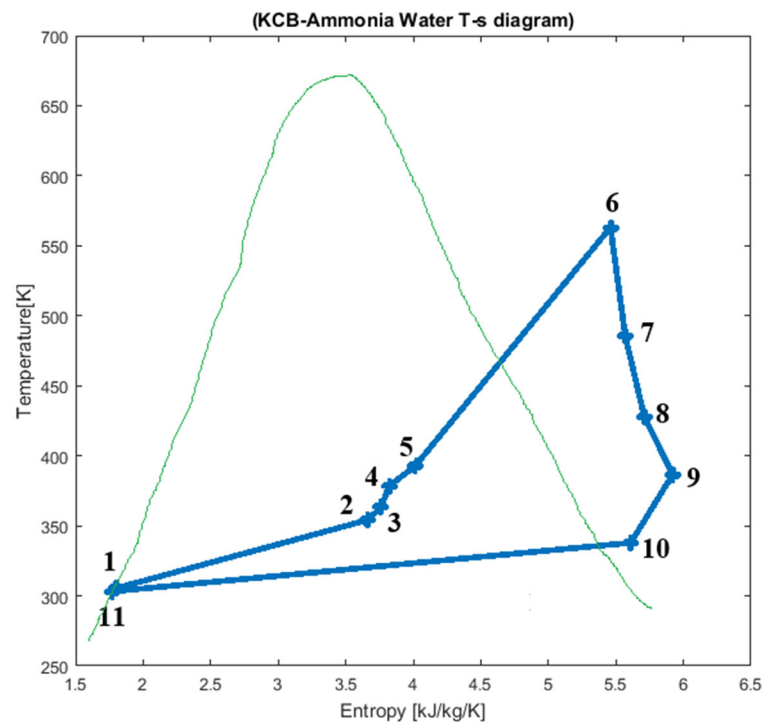
Figure 3. Exergy destruction rate of different components: (**a**) KCA, (**b**) KCB, and (**c**) KCC.

Figure 4. *Cont.*

(**B**)
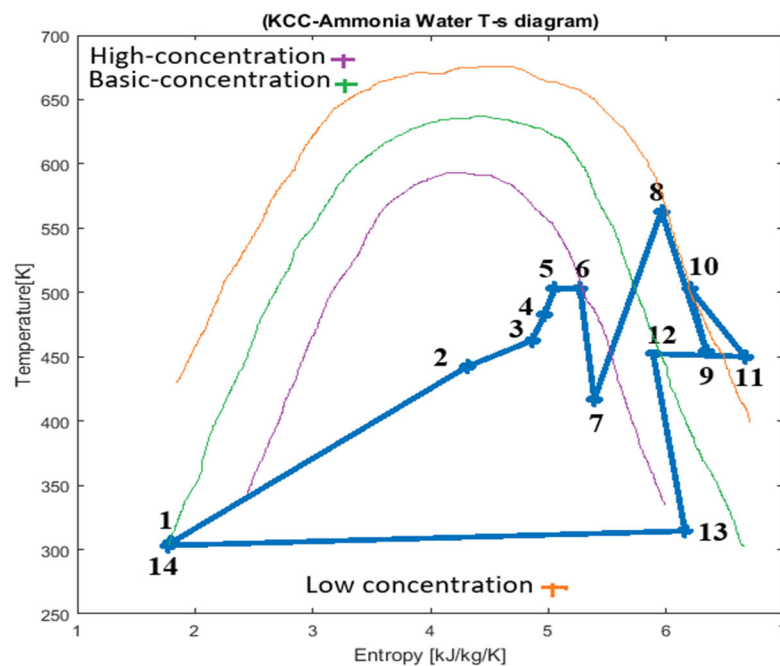
(**C**)

Figure 4. T–s diagrams of KCA (**A**), KCB (**B**), and KCC (**C**).

3.1. Effect of the Inlet Temperature of the High-Pressure Turbine (HPT)

The effect of varying the inlet temperature of the high-pressure turbine on energy efficiency and performance is examined in Figure 5. The study was conducted in a temperature range between 200 °C and 360 °C, with an increment of 20 °C. Figure 5 presents the variation of specific performance electrical and mechanical powers, and thermal efficiency when the inlet temperature of the HPT high-pressure turbine changes. At first sight, the curves of Figure 5 present a similarity regarding their paces. Figure 5a shows that the

KCA and KCC systems provide almost similar work and are superior to the KCB system. However, an important observation is that at the lowest temperature, it is the KCA system that presents the highest specific work. As soon as the temperature of 250 °C is reached, the KCC system takes over, presenting the highest specific work.
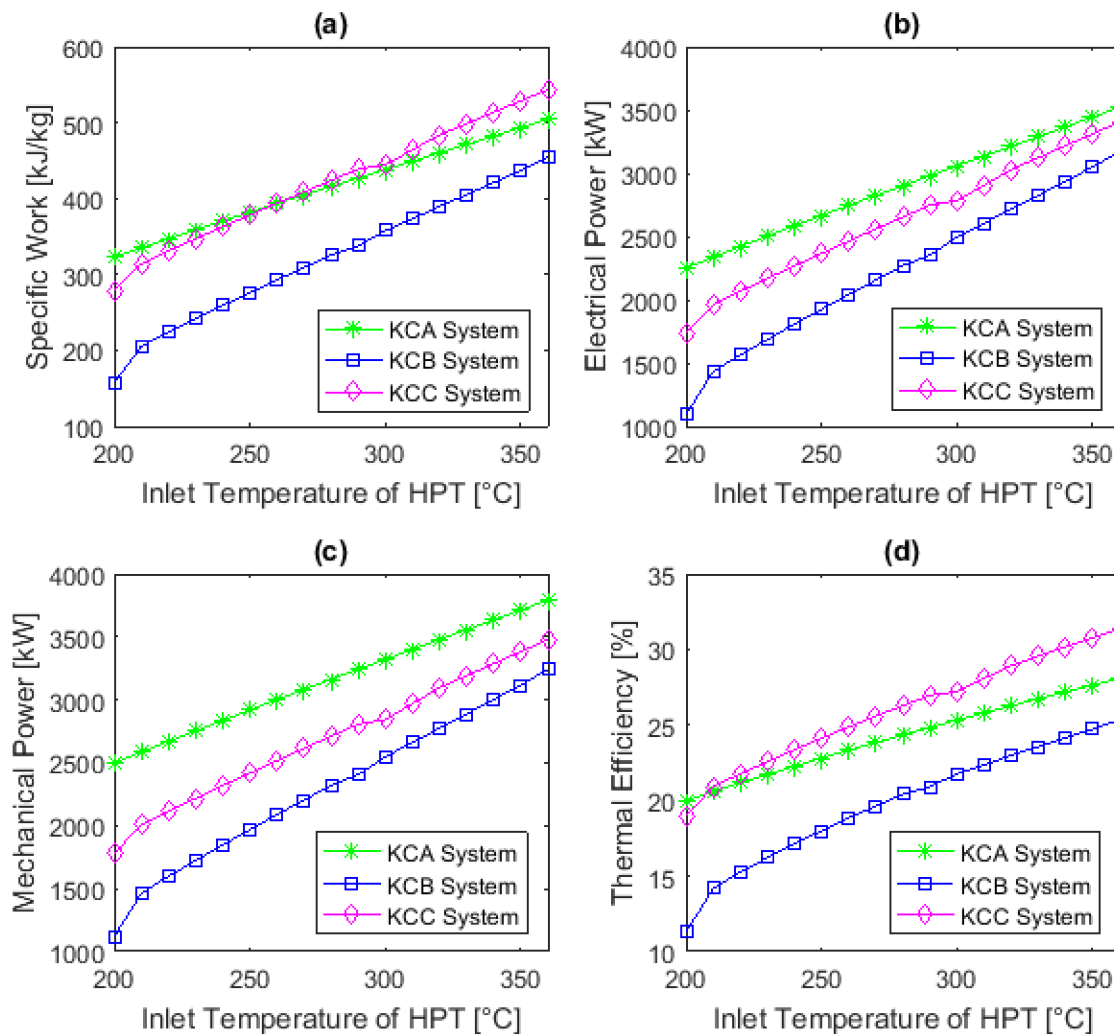

Figure 5. Effect of the inlet temperature of HPT on the: (**a**) specific performance, (**b**) electrical power, (**c**) mechanical power, and (**d**) thermal efficiency.

A similar observation is made for thermal efficiency (Figure 5d). This time the KCA system has the best thermal efficiency between 200 °C and 215 °C. At 215 °C, the KCC system shows the best thermal efficiency. Overall, the KCC system has better thermal efficiencies than the KCA and KCB systems. This can be explained by the presence of a separator, which allows the turbines to suck only in the vapor phase, unlike the other two systems, KCA and KCB, where all the mixture enters directly into the high-pressure turbine without undergoing a prior separation. The separator raises the ammonia concentration to 0.9 at the inlet of HPT and HPB, while for systems without a separator (KCA and KCB), the ammonia concentration is only 0.88. According to Equation (1), the increase in ammonia concentration leads to an increase in enthalpy at the inlet of the high-pressure turbine, increasing the specific work. For a given temperature, the enthalpy of ammonia is close at a given point for all the systems studied. Therefore, only the concentration of ammonia creates the difference between these cycles. In general, the temperature increase leads to an increase in specific work and thermal efficiency.

The KCA system exhibits high electrical power compared to the other two systems (Figure 5b). The same observation is valid for the evolution of mechanical power (Figure 5c). The shapes of the curves of Figure 5b,c are quasi-parallel and similar, which is expected. After fixing the isentropic, mechanical, and electrical efficiencies, the electrical power depends only on the turbine rotor shaft (mechanical) power. Increasing the steam's temperature at the turbine inlet increases the turbine's enthalpy, which increases the net power generated.

Figure 6 presents the electrical and mechanical power curves and the specific work when the thermal efficiency varies, following the temperature variation at the inlet of the high-pressure turbine. The thermal efficiency being a function of the temperature, its influence in the Kalina cycles should not be neglected. By varying the temperature between 200 °C and 360 °C, the thermal efficiency also varies from 19.99 to 28.08% for the KCA system, from 11.27 to 25.35% for the KCB system, and from 18.98 to 31.37% for the KCC system. For high thermal efficiency values, the mechanical power is 3793.49 kW, 3241.78 kW, and 3478.71 KW, respectively, for the KCA, KCB, and KCC systems (Figure 6a). Electrical powers are 3521.18 kW, 3172.98 kW, and 3405.17 kW, respectively, for the KCA, KCB, and KCC systems (Figure 6b). Finally, the specific work is 504.50 kJ/kg, 454.66 kJ/kg, and 543.37 kJ/kg, respectively, for the KCA, KCB, and KCC systems (Figure 6c). Given the above, the KCA system presents the best results regarding mechanical and electrical power and specific performance.
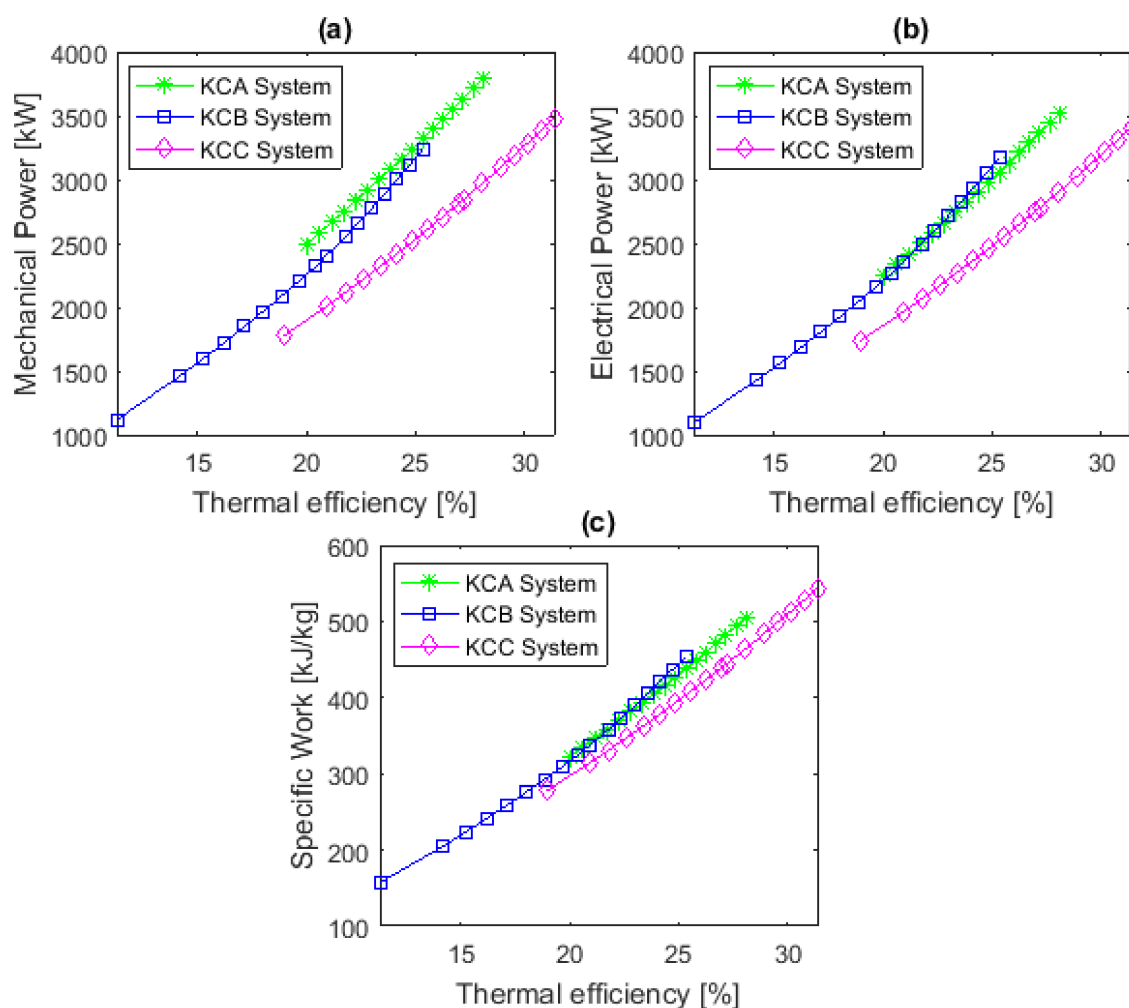

Figure 6. Influence of thermal efficiency (under the effect of inlet temperature of HPT) on the: (**a**) mechanical power, (**b**) electrical power, (**c**) specific performance.

3.2. *Effect of the Pump Discharge Pressure*

The effect of varying pump discharge pressure (or high-pressure turbine inlet pressure) on the performance of the three systems is illustrated in Figures 7 and 8. The mass fraction of the ammonia at the high-pressure turbine inlet was maintained at 88% for all systems. The exception is the KCC system, where the 88% NH_3 concentration first passes through a separator before entering the high-pressure turbine. At the outlet of the separator (point six), the NH_3 concentration is 90% (rich mixture) at the inlet of the high-pressure turbine. Figure 7a shows the effect of pressure variation on specific work. The specific work increases with pressure, between 3 and 11 MPa for the KCA system, between 3 and 15 MPa for the KCB system, and between 3 and 9 MPa for the KCC system. Afterward, the specific performance decreases with the pressure increase up to 19 MPa. When the pressure is low, the specific performance curve of the KCC system is higher than the KCA and KCB systems. As soon as the evaporating pressure reaches the value of 7 MPa, the curve of the KCA system takes over. Thus, there is a shift in favor of the KCA system, although the specific performance of the KCC system continues to increase. The same phenomenon is observed for the electrical and mechanical power cases (see Figure 7b,c). The effect of the evaporation pressure on the different Kalina cycles' electrical power is illustrated in Figure 7b. As for the specific work, an electrical power peak occurs with a pressure increase: 3132.12 kW at around 12 MPa for the KCA system, 2501.50 kW at around 12 MPa for the KCB, and 3061.59 kW at 9 MPa for KCC. Then, the electrical power gradually decreases as the pressure increases. Similar observations are valid for the mechanical power and the thermal efficiency of the Kalina cycles (Figure 7c,d).
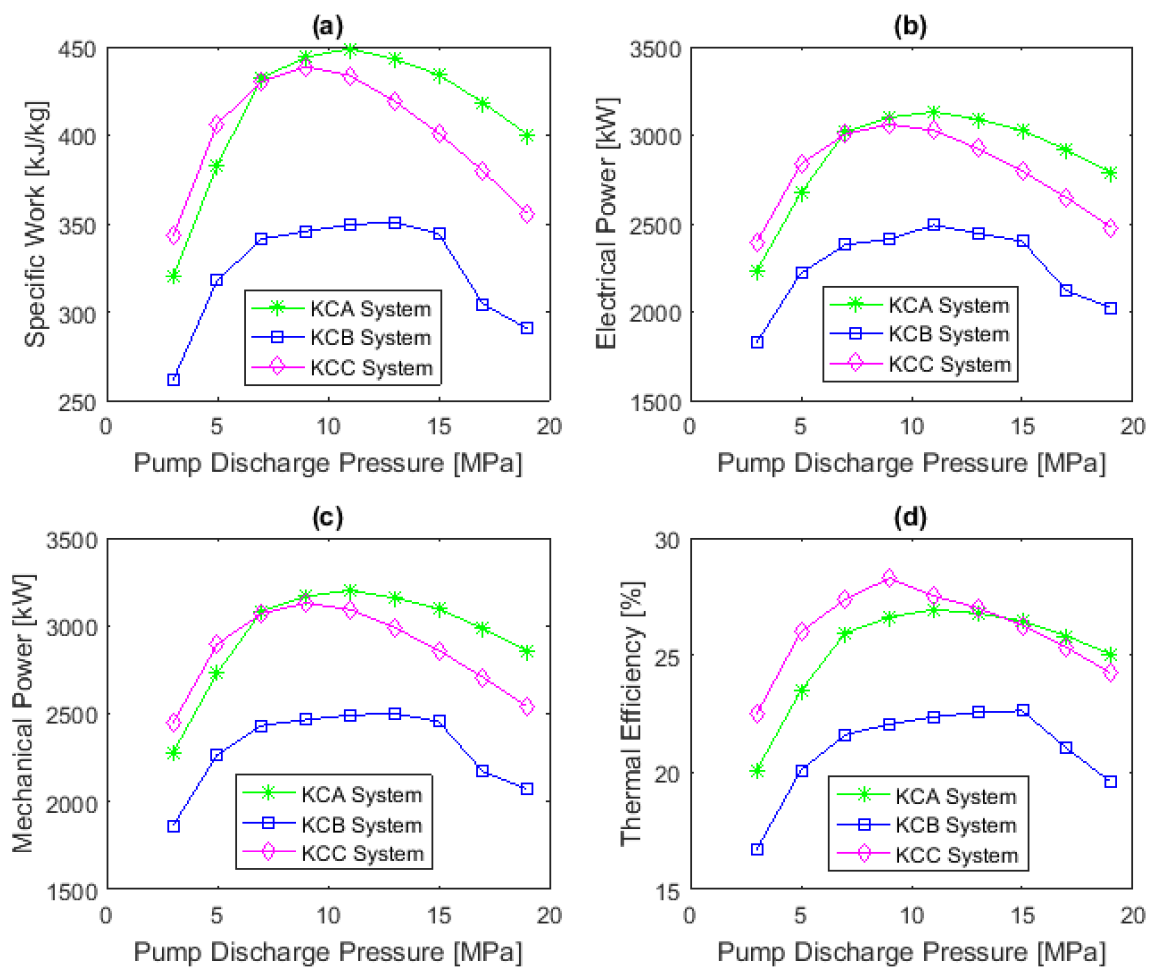

Figure 7. Effect of pump discharge pressure on the: (**a**) specific performance, (**b**) electrical power, (**c**) mechanical power, and (**d**) thermal efficiency.
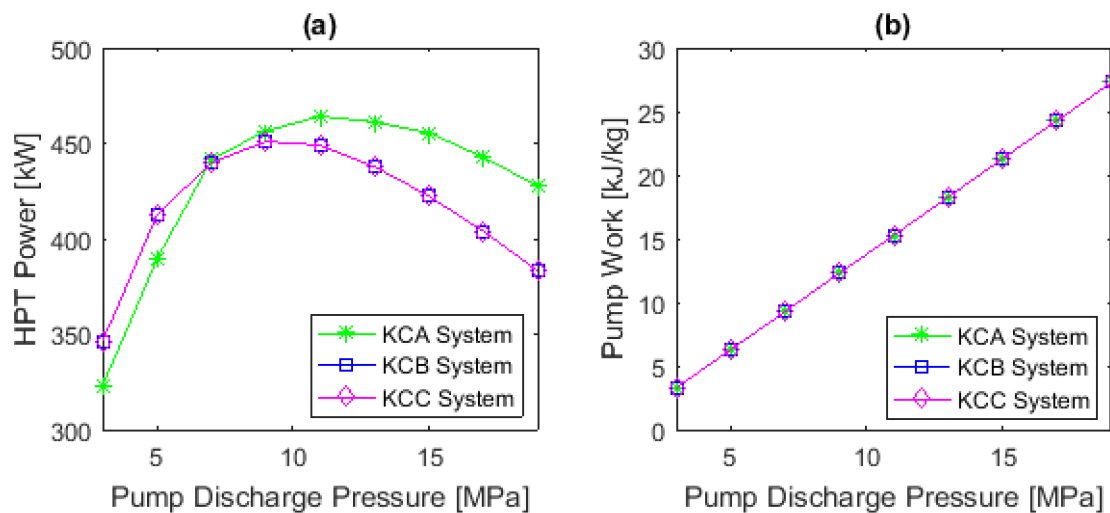
Figure 8. Effect of pump discharge pressure on the: (**a**) HPT power and (**b**) pump performance.

We notice mechanical power peaks at 12 MPa for the KCA system (3200.53 kW), at about 15 MPa for the KCB system (2501.499 kW), and 9 MPa (3127.68 kW) for the KCC system. The best thermal efficiency is 26.93% at 12 MPa (for KCA), 22.62% at 15 MPa (for KCB), and 31.28% at 9 MPa (for KCC), respectively. KCA and KCC systems perform better than KCB systems when the pressure varies. The performance of the KCB system, although having three turbines, is very low compared to the other two. However, the KCB system can be improved by placing the second superheater between the high-pressure turbine and the medium-pressure turbine or between the medium-pressure turbine and the low-pressure turbine.

Figure 7d presents a particularity compared to Figure 7a–c. The thermal efficiency curve of the KCC system is superior to the KCA systems on both the increasing and decreasing sides of the curve. The shift in favor of the KCA system only occurs when the pressure reaches a value of about 14 MPa (on the decay side of the curve). Overall, by increasing the pressure, the KCC model gives better thermal efficiencies than the other models. Once again, the presence of the separator in the KCC model is the basis for this performance.

In Figure 8, it appears that as the evaporating pressure increases, the trend in the variation in turbine power is consistent with that of the net power output. In addition, the pump work increases linearly with the increasing pressure. Concerning the power of the high-pressure turbine (Figure 8a), the curve shapes are like those of the specific performance and the electrical and mechanical powers (Figure 7a–c). For a discharge pressure variation from 3 to 19 MPa, the curves of the pump work of the three systems are superimposed. This is explained by the fact that the pumps receive the same flow rate of the ammoniacal solution from the condenser at an atmospheric pressure.

3.3. Effect of NH$_3$ Concentration

Figure 9 illustrates the influence of the ammonia concentration on the performance of Kalina cycles. The study concerns ammonia concentrations between 60% and 94%. Figure 8a shows that the specific performance increases with the ammonia concentration as the higher ammonia concentration increases the heat transfer rate in the evaporator. This increase differs from one cycle to another. The KCA and KCB cycles present a slight slope, whereas the increase in the specific performance of the KCC cycle is very accentuated. The presence of the separator in the KCC system means that the specific work can increase rapidly compared to the other two systems. The concentration of NH$_3$ entering the separator (point five) is increased at the turbine inlet (point six). As the increase in the concentration of ammonia NH$_3$ leads to an increase in the enthalpy (see Equation (1)), the specific performance of the KCC system varies considerably compared to the other two cases. This phenomenon is also noticeable in Figure 9b–d.
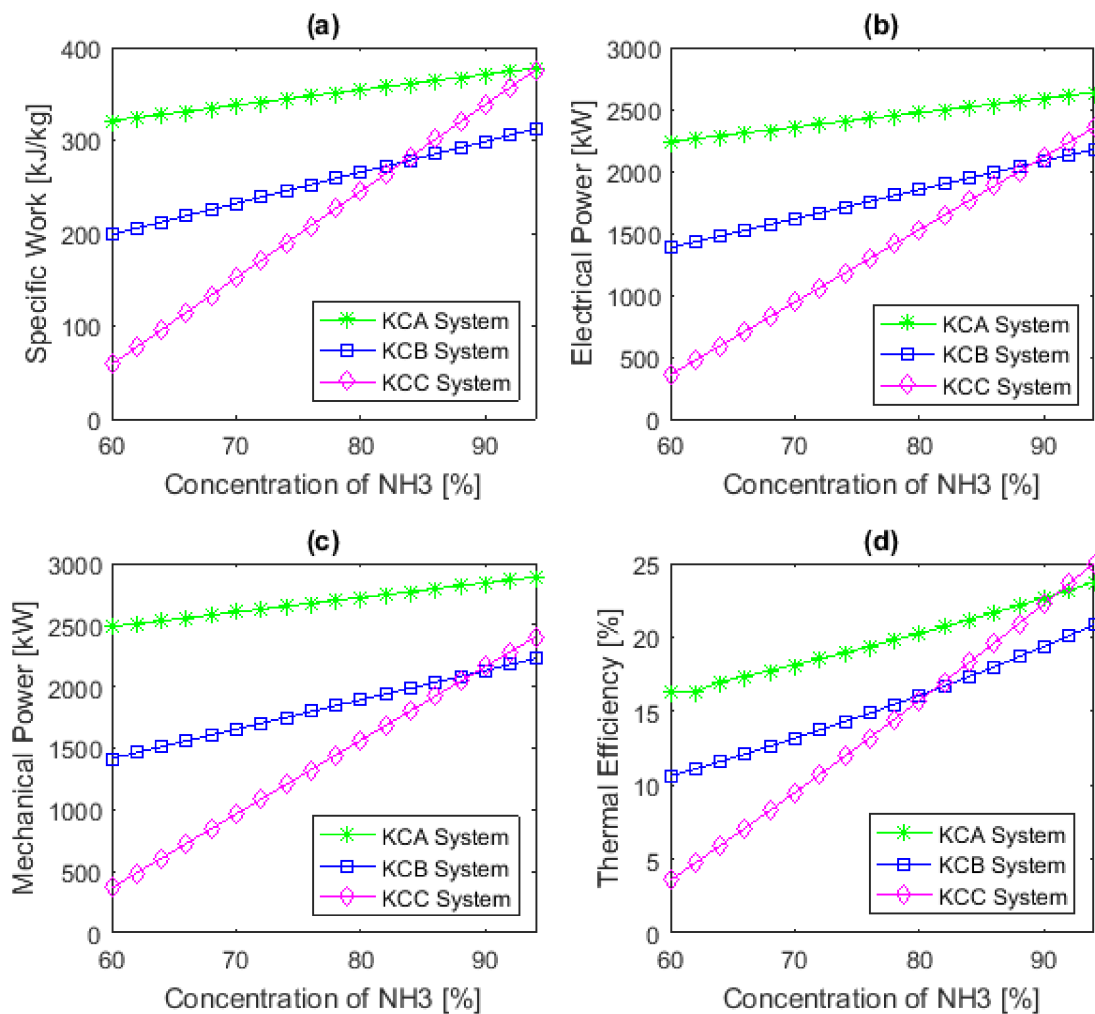
Figure 9. Effect of NH_3 concentration on the: (**a**) specific performance, (**b**) electrical power, (**c**) mechanical power, and (**d**) thermal efficiency.

Figure 9b,c show the electrical and mechanical power variations with the ammonia concentrations. The figures highlight the increased electrical and mechanical powers with the concentration under the optimum evaporation pressure. The variation in NH_3 concentration affects the mass flow and increases the value of the net power generated in the cycle. This behavior is because the mixture richer in ammonia boils faster, resulting in a higher steam generation, increasing the power generated in the high-pressure turbine.

The influence of the NH_3 concentration on thermal efficiencies is given in Figure 9d. The latter shows that the KCA system performs better than the other two. The KCC system is less efficient than the KCA and KCB systems. For concentrations higher than 81.5%, the KCC system becomes more efficient than the KCB system. With over 91% NH_3 concentration, the KCC becomes the most efficient system compared to the KCA and KCB. Thus, there is an improvement in the thermal efficiency of the KCC model. As mentioned, in the KCC system, the NH_3 concentration varies twice before entering the high-pressure turbine. As a result, the thermal efficiency curve increases faster than for the KCA and KCB systems. Similar to Figure 9a, the slopes of the electrical power (Figure 9b), mechanical power (Figure 9c), and thermal efficiency (Figure 9c) of the cycle KCC are also very accentuated.

3.4. Validation of the Results

We used comparable studies in the literature to validate this model, as no results are available for similar conditions and cycle configurations. Therefore, the comparisons are made using the results of the KCA system (see Table 7). First, we identified previous work

with comparable operating parameters (input data), and we selected the two references in Table 12. Then, the service temperature, thermal efficiency, exergetic efficiency, and net electrical power were retained as the key parameters to be compared. Our results are comparable with those of Júnior et al. [13] and Da costa Horta [19], especially for thermal and exergetic efficiency. As for electrical power, the prediction of this model is very close to that of Júnior et al. [13] (see Table 13). Overall, the predictions of the model of Júnior et al. [13] are very close to those of this model, although the temperature is slightly higher.

Table 12. Inlet data for validation.

Operating Parameters	Júnior et al. [13]	Da costa Horta [19]	Present Model
Turbine isentropic efficiency	85%	85%	85%
Pump isentropic efficiency	85%	70%	85%
Ambient temperature	22 °C	15 °C	30 °C
Ambient pressure	101.325 kPa	101.325 kPa	101.325 kPa
Pinch point	18 K	10 K	10 K
Temperature of cooling water	-	22 °C	20 °C
Concentration of ammonia–water solution	89%	88.6%	88%

Table 13. Comparison with different results in the literature.

Parameters	Júnior et al. [13]	Da costa Horta [19]	Present Model
Temperature [°C]	390	340	300
Thermal efficiency [%]	23.3	25.1	22.15
Exergetical efficiency [%]	47.8	55.8	40.35
Net electrical power [kWe]	2429.056	10,493.9	2565.03

The simulation errors compared with the results of the work of Júnior et al. [13] are presented in Table 14.

Table 14. Error in the simulation.

Parameters	Júnior et al. [13]	Present Model	Error %
Temperature [°C]	390	300	23.08
Thermal efficiency [%]	23.3	22.15	4.94
Exergetical efficiency [%]	47.8	40.35	15.59
Net electrical power [kWe]	2429.056	2565.03	5.60

Because of the above, this model's results can be considered reliable and valid.

4. Conclusions and Perspectives

Three new Kalina cycles have been studied for energy performance. These cycles include two to three turbines and two superheaters, aiming to increase the system's efficiency and thus allow the turbines to work only in the vapor phase. There are two levels of energy recovery: the hot gases exiting the preheater tower and those exiting the clinker cooler chimney. This study aims to recover the waste heat in the gases leaving the cement rotary kiln via cogeneration. The Kalina cycles are studied and evaluated in the context of the production of both heat and electricity. The KCA system presented the best results for the electrical power generated, the mechanical power, and the specific work. It also showed better efficiencies (a thermal efficiency of 22.15% and an exergy efficiency of 45.12%). The

model's sensitivity to concentration, temperature, and pressure variations also gave the KCA system the best-performing system. Yet when the pressure starts to vary, the KCC model gives the best performance in terms of thermal efficiencies (see Figure 7d). A similar observation can be made when the NH_3 concentration varies (Figure 9d), where the thermal efficiency of the KCC model is best for NH_3 concentrations above 91%.

The maximum electrical power of the KCA system, found by varying the pressure, reaches 3132.12 kW, while for the KCB and KCC systems it is 2501.50 kW and 3061.59 kW, respectively. When the temperature at the inlet of the high-pressure turbine varies, the KCA system is still the best. It can generate a maximum power of 3521.18 kW, followed by the KCC system, with 3405.17 kW. Finally, the KCB system is the worst, with an electrical power of 3172.98 kW. We also studied the influence of the ammonia concentration on the different cycles.

Nevertheless, the KCA system still has the best performance. The Kalina cycles proposed in this research can be extended and implemented for other applications such as trigeneration. The mathematical model presented in this research can be used for these purposes. Although the configurations studied in this article give acceptable results, it is essential to analyze the system's critical parameters in detail. Additional assumptions can reduce the complexity of the study. The studies in progress concern the coupling of the KCA system with an absorption diffusion refrigeration cycle within the framework of trigeneration.

Author Contributions: Conceptualization, M.T.M.; Methodology, B.-J.R.M.B., A.I. and M.T.M.; Software, B.-J.R.M.B.; Validation, A.I.; Formal analysis, L.M.M.; Resources, M.T.M. and L.M.M. Data curation, B.-J.R.M.B.; Writing—review & editing, B.-J.R.M.B.; Visualization, M.T.M. and L.M.M.; Supervision, B.-J.R.M.B.; Project administration, A.I.; Funding acquisition, A.I. All authors have read and agreed to the published version of the manuscript.

Conflicts of Interest: The authors declare that they have no known competing financial interest or personal relationship that could have appeared to influence the work reported in this paper.

Abbreviations

Latin letters

Symbol	Signification	Unit
A	Heat transfer surface area	m^2
$\dot{E}x$	Primary exergy	kJ
ex	Specific exergy	kJ/kg
F_i	Dimensional factor	-
h	Specific enthalpy	kJ/kg
$h_{iKalina}$	Enthalpy of the mixture at point i (i = 1 to the number of points in the cycle)	kJ/kg
h_{NH3i}	Enthalpy of ammonia in the mixture at the point i	kJ/kg
$h_{H_2O\ i}$	Enthalpy of the water vapor in the mixture at point i	kJ/kg
h_i	Heat transfer global coefficient	$kW/m^2/K$
$\dot{m}$	Mass flow rate	kg/s
$\dot{Q}$	Themal power	kW
$\dot{q}_i$	Heat transfer rate of exhausted gas	kW
s	Specific entropy	kJ/kg/K
T	Temperature	K
T_{gsor}	Exit gas temperature	K
ΔT	Variation of temperature	K
$\dot{w}$	Work per time unit	kJ/s
x_{NH3}	Concentration of ammonia in the mixture	%

Greek letters

η	Efficiency	%

Subscripts

cond	Condenser
evap	Evaporator
gcol	Gas from cooler
*gcol*1	Gas from cooler before heat exchanger 2
*gcol*2	Gas from cooler after heat exchanger 2
gcy	Gas from cyclone
*gcy*1	Gas from cyclone before heat exchanger 1
*gcy*2	Gas from cyclone after heat exchanger 1
*HEX*1	Heat exchanger 1
*HEX*2	Heat exchanger 2
HR	Heat recovery amount from this process
*HR*1	Heat recovery 1
*HR*2	Heat recovery 2
In	Inlet
isHPT	Isentropic, high-pressure turbine
isLPT	Isentropic, low-pressure turbine
isPump	Isentropic pump
LMTD	Due to the logarithmic mean temperature difference
Out	Outlet
P	Pump
preh	Preheater
*pump*1	Feed pump 1
*pump*2	Feed pump 2
Rec	Heat recovered amount in the regenerator
*superh*1	Superheater 1
*superh*2	Superheater 2
T	Turbine
0	Ambient condition

Superscripts

D	Refers to exergy destruction
Q	Concerned with heat transfer
W	Concerned with power

Abbreviations

HPT	High-pressure turbine
IEA	International energy agency
KCA	Kalina cycle (A)
KCB	Kalina cycle (B)
KCC	Kalina cycle (C)
LNG	Liquefied natural gas
LPT	Low-pressure turbine
MPT	Medium-pressure turbine
N.A.	Not applicable
ORC	Organic Rankine cycle
RDF	Refuse-derived fuel

References

1. Bisulandu, B.-J.R.M.; Marias, F. Modeling of the Thermochemical Conversion of Biomass in Cement Rotary Kiln. *Waste Biomass Valorization* **2021**, *12*, 1005–1024. [CrossRef]
2. Mujumdar, K.; Ranade, V. Simulation of Rotary Cement Kilns Using a One-Dimensional Model. *Chem. Eng. Res. Des.* **2006**, *84*, 165–177. [CrossRef]
3. Bisulandu, B.J.R.M.; Pongo, P. Les énergies renouvelables face à l'épuisement des énergies fossiles: Utilisation et Valorisation des déchets dans les fours de cimenterie. In *Septième Édition du COlloque FRancophone en Energie, Environnement, Economie et Thermodynamique-COFRET'14*, 7th ed.; COFRET: Paris, France, 2014; pp. 905–918.
4. Jalalizadeh, M.; Fayaz, R.; Delfani, S.; Mosleh, H.J.; Karami, M. Dynamic simulation of a trigeneration system using an absorption cooling system and building integrated photovoltaic thermal solar collectors. *J. Build. Eng.* **2021**, *43*, 102482. [CrossRef]

5.　Jamaluddin, K.; Alwi, S.R.W.; Manan, Z.A.; Hamzah, K.; Klemeš, J.J. Design of Total Site-Integrated TrigenerationSystem using trigeneration cascade analysis considering transmission losses and sensitivity analysis. *Energy* **2022**, *252*, 123958. [CrossRef]

6.　Haghanimanesh, M.; Baniasadi, E.; Kerdabadi, J.K.; Yu, X. Exergoeconomic analysis of a novel trigeneration cycle based on steel slag heat recovery and biogas production in steelmaking plants. *Energy Convers. Manag.* **2022**, *263*, 115688. [CrossRef]

7.　Ma'Aji, N.S.; Adun, H.; Shefik, A.; Adedeji, M.; Dagbasi, M. Design of trigeneration plant for electricity freshwater production, and district heating: A case study Periwinkle Lifestyle Estate, Lagos Nigeria. *Case Stud. Therm. Eng.* **2022**, *35*, 102041. [CrossRef]

8.　Roy, D.; Samanta, S. Development and multiobjective optimization of a novel trigeneration system based on biomass energy. *Energy Convers. Manag.* **2021**, *240*, 114248. [CrossRef]

9.　Jana, K.; Ray, A.; Majoumerd, M.M.; Assadi, M.; De, S. Polygeneration as a future sustainable energy solution—A comprehensive review. *Appl. Energy* **2017**, *202*, 88–111. [CrossRef]

10.　Guillén-Lambea, S.; Pina, E.; Serra, L.; Lozano, M.; Lazaro, A. Environmental assessment of medium-size solar organic Rankine Cycle cogeneration plants. *Appl. Therm. Eng.* **2022**, *213*, 118692. [CrossRef]

11.　Douvartzides, S.L.; Tsiolikas, A.; Charisiou, N.D.; Souliotis, M.; Karayannis, V.; Taousanidis, N. Energy and Exergy-Based Screening of Various Refrigerants, Hydrocarbons and Siloxanes for the Optimization of Biomass Boiler–Organic Rankine Cycle (BB–ORC) Heat and Power Cogeneration Plants. *Energies* **2022**, *15*, 5513. [CrossRef]

12.　Atănăsoae, P. Allocation of Joint Costs and Price Setting for Electricity and Heat Generated in Cogeneration. *Energies* **2022**, *16*, 134. [CrossRef]

13.　Júnior, E.P.B.; Arrieta, M.D.P.; Arrieta, F.R.P.; Silva, C.H.F. Assessment of a Kalina cycle for waste heat recovery in the cement industry. *Appl. Therm. Eng.* **2019**, *147*, 421–437. [CrossRef]

14.　Varma, G.P.; Srinivas, T. Parametric Analysis of Steam Flashing in a Power Plant Using Waste Heat of Cement Factory. *Energy Procedia* **2016**, *90*, 99–106. [CrossRef]

15.　Salemi, S.; Torabi, M.; Haghparast, A.K. Technoeconomical investigation of energy harvesting from MIDREX® process waste heat using Kalina cycle in direct reduction iron process. *Energy* **2022**, *239*, 122322. [CrossRef]

16.　Inayat, A. Current progress of process integration for waste heat recovery in steel and iron industries. *Fuel* **2023**, *338*, 127237. [CrossRef]

17.　Cheng, Z.; Wang, J.; Yang, P.; Wang, Y.; Chen, G.; Zhao, P.; Dai, Y. Comparison of control strategies and dynamic behaviour analysis of a Kalina cycle driven by a low-grade heat source. *Energy* **2022**, *242*, 122958. [CrossRef]

18.　Hossain, M.M.; Hossain, S.; Ahmed, N.A.; Ehsan, M.M. Numerical Investigation of a modified Kalina cycle system for high-temperature application and genetic algorithm based optimization of the multi-phase expander's inlet condition. *Energy AI* **2021**, *6*, 100117. [CrossRef]

19.　Horta, G.R.D.C.; Barbosa, E.P.; Moreira, L.F.; Arrieta, F.R.P.; de Oliveira, R.N. Comparison of Kalina cycles for heat recovery application in cement industry. *Appl. Therm. Eng.* **2021**, *195*, 117167. [CrossRef]

20.　Zheng, S.; Chen, K.; Du, Y.; Fan, G.; Dai, Y.; Zhao, P.; Wang, J. Comparative analysis on off-design performance of a novel parallel dual-pressure Kalina cycle for low-grade heat utilization. *Energy Convers. Manag.* **2021**, *234*, 113912. [CrossRef]

21.　Akimoto, R.; Yamaki, T.; Nakaiwa, M.; Matsuda, K. Evaluation of a power generation system that integrates multiple Kalina cycles and absorption heat pumps. *Case Stud. Therm. Eng.* **2021**, *28*, 101363. [CrossRef]

22.　Roeinfard, N.; Moosavi, A. Thermodynamic analysis and optimization of the organic Rankine and high-temperature Kalina cycles for recovering the waste heat of a bi-fuel engine. *Fuel* **2022**, *322*, 124174. [CrossRef]

23.　Zhang, S.; Hao, X.; Chen, Y.; Wu, J. Thermodynamic study on power and refrigeration cogeneration Kalina cycle with adjustable refrigeration temperature. *Int. J. Refrig.* **2021**, *131*, 706–713. [CrossRef]

24.　Almatrafi, E.; Khaliq, A.; Alquthami, T. Thermodynamic investigation of a novel cooling-power cogeneration system driven by solar energy. *Int. J. Refrig.* **2022**, *138*, 244–258. [CrossRef]

25.　Zhang, X.; Li, Z. Performance of Kalina cycle with single-screw expander for low-temperature geothermal energy utilization. *Appl. Therm. Eng.* **2022**, *210*, 118364. [CrossRef]

26.　Zhu, H.; Xie, G.; Yuan, H.; Nizetic, S. Thermodynamic assessment of combined supercritical CO2 cycle power systems with organic Rankine cycle or Kalina cycle. *Sustain. Energy Technol. Assess.* **2022**, *52*, 102166. [CrossRef]

27.　Zoghi, M.; Habibi, H.; Chitsaz, A.; Holagh, S.G. Multi-criteria analysis of a novel biomass-driven multi-generation system including combined cycle power plant integrated with a modified Kalina-LNG subsystem employing thermoelectric generator and PEM electrolyzer. *Therm. Sci. Eng. Prog.* **2021**, *26*, 101092. [CrossRef]

28.　Aksar, M.; Yağlı, H.; Koç, Y.; Koç, A.; Sohani, A.; Yumrutaş, R. Why Kalina (Ammonia-Water) cycle rather than steam Rankine cycle and pure ammonia cycle: A comparative and comprehensive case study for a cogeneration system. *Energy Convers. Manag.* **2022**, *265*, 115739. [CrossRef]

29.　Zhang, X.; He, M.; Zhang, Y. A review of research on the Kalina cycle. *Renew. Sustain. Energy Rev.* **2012**, *16*, 5309–5318. [CrossRef]

30.　Ogriseck, S. Integration of Kalina cycle in a combined heat and power plant, a case study. *Appl. Therm. Eng.* **2009**, *29*, 2843–2848. [CrossRef]

31.　Mirolli, M. The Kalina cycle for cement kiln waste heat recovery power plants. In Proceedings of the Conference Record Cement Industry Technical Conference 2005, Kansas City, MO, USA, 15–20 May 2005; pp. 330–336.

32. Mirolli, M. Ammonia-water based thermal conversion technology: Applications in waste heat recovery for the cement industry. In Proceedings of the 2007 IEEE Cement Industry Technical Conference Record, Charleston, SC, USA, 29 April–2 May 2007; pp. 234–241.

33. Braimakis, K.; Karellas, S. Exergy efficiency potential of dual-phase expansion trilateral and partial evaporation ORC with zeotropic mixtures. *Energy* **2023**, *262*, 125475. [CrossRef]

34. Ustaoglu, A.; Alptekin, M.; Akay, M.E. Thermal and exergetic approach to wet type rotary kiln process and evaluation of waste heat powered ORC (Organic Rankine Cycle). *Appl. Therm. Eng.* **2017**, *112*, 281–295. [CrossRef]

35. Karellas, S.; Leontaritis, A.-D.; Panousis, G.; Bellos, E.; Kakaras, E. Energetic and exergetic analysis of waste heat recovery systems in the cement industry. *Energy* **2013**, *58*, 147–156. [CrossRef]

36. Rad, E.A.; Mohammadi, S. Energetic and exergetic optimized Rankine cycle for waste heat recovery in a cement factory. *Appl. Therm. Eng.* **2018**, *132*, 410–422.

37. Piri, A.; Aghanajafi, C.; Sohani, A. Enhancing efficiency of a renewable energy assisted system with adiabatic compressed-air energy storage by application of multiple Kalina recovery cycles. *J. Energy Storage* **2023**, *61*, 106712. [CrossRef]

38. Khalid, F.; Dincer, I.; Rosen, M.A. Energy and exergy analyses of a solar-biomass integrated cycle for multigeneration. *Sol. Energy* **2015**, *112*, 290–299. [CrossRef]

39. Pietrasanta, A.M.; Mussati, S.F.; Aguirre, P.A.; Morosuk, T.; Mussati, M.C. Optimization of Cogeneration Power-Desalination Plants. *Energies* **2022**, *15*, 8374. [CrossRef]

40. Kalan, A.S.; Heidarabadi, S.; Khaleghi, M.; Ghiasirad, H.; Skorek-Osikowska, A. Biomass-to-energy integrated trigeneration system using supercritical CO_2 and modified Kalina cycles: Energy and exergy analysis. *Energy* **2023**, *270*, 126845. [CrossRef]

41. Bontemps, A.; Garrigue, A.; Goubier, C. Technologie des échangeurs thermiques. In *Techniques de L'ingénieur Groupement pour la Recherche sur les Échangeurs Thermiques*; Techniques de l'Ingenieur: Paris, France, 1998.

42. Liu, X.; Hu, G.; Zeng, Z. Performance characterization and multi-objective optimization of integrating a biomass-fueled brayton cycle, a kalina cycle, and an organic rankine cycle with a claude hydrogen liquefaction cycle. *Energy* **2023**, *263*, 125535. [CrossRef]

43. Dincer, I.; Rosen, M.A. Chapter 2—Exergy and Energy Analyses. In *Exergy*, 2nd ed.; Dincer, I., Rosen, M.A., Eds.; Elsevier: Amsterdam, The Netherlands, 2013; pp. 21–30. [CrossRef]

44. Ahmadi, P.; Dincer, I.; Rosen, M.A. Energy and exergy analyses of hydrogen production via solar-boosted ocean thermal energy conversion and PEM electrolysis. *Int. J. Hydrogen Energy* **2013**, *38*, 1795–1805. [CrossRef]

45. Ahmadi, P.; Dincer, I. Thermodynamic and exergoenvironmental analyses, and multi-objective optimization of a gas turbine power plant. *Appl. Therm. Eng.* **2011**, *31*, 2529–2540. [CrossRef]

46. Ahmadi, P.; Dincer, I.; Rosen, M.A. Exergo-environmental analysis of an integrated organic Rankine cycle for trigeneration. *Energy Convers. Manag.* **2012**, *64*, 447–453. [CrossRef]

47. Dincer, I.; Hussain, M.; Al-Zaharnah, I. Energy and exergy utilization in transportation sector of Saudi Arabia. *Appl. Therm. Eng.* **2004**, *24*, 525–538. [CrossRef]

48. Bejan, A.; Tsatsaronis, G.; Moran, M.J. *Thermal Design and Optimization*; John Wiley & Sons: New York, NY, USA, 1996.